American Mineralogist, Volume 91, pages 1163–1169, 2006

Mössbauer characterization of upper mantle ferrikaersutite

SOBHI NASIR[1,*] AND AHMAD D. AL-RAWAS[2]

[1]Department of Earth Science, Sultan Qaboos University, 123 Al-Khod, Oman
[2]Department of Physics, Sultan Qaboos University, 123 Al-Khod, Oman

ABSTRACT

Mössbauer spectroscopy, H_2O, and microprobe analysis techniques have been used to study upper mantle ferrikaersutite megacrysts from the scoria cones of the Ash Sham alkaline volcanic field, northeastern part of the Arabian plate. Mössbauer spectra, collected at 298 K, indicate that the kaersutites are highly oxidized and all iron occurs as Fe^{3+}. Two components were detected within the Fe^{3+} quadrupole splitting distribution of the C-type sites and were assigned to M1 and M2-3 sites. The quadrupole splitting (QS) varies between 0.73–0.87 mm/s (Fe^{3+} M1) and 1.28–1.45 mm/s (Fe^{3+} M2-3). The kaersutite has a large oxy component in the amphibole OH-site (1.49–1.85 O^{2-} apfu) similar to the mantle-derived kaersutites. The very high ferric concentration in the kaersutites would suggest crystallization from a relatively oxidizing magma, perhaps with f_{O_2} close to the fayalite-magnetite-quartz (FMQ), and may be a function of the high Fe^{3+}/Fe_{tot} of the metasomatic fluid that crystallized these amphiboles.

Keywords: Mössbauer, microprobe, ferrikaersutite, upper mantle, Arabian plate, oxidation, metasomatism

INTRODUCTION

Kaersutite, $NaCa_2[(Mg,Fe^{2+})_4Ti](Si_6Al_2)O_{23}(OH)$ belongs to the calcic subgroup of amphiboles (Leake et al. 1997). It is formed through crystallization from mafic-ultramafic melts at low to moderate pressure (≤1.0 GPa), high temperature (>950 °C) and low to moderate oxygen fugacity (Allen and Boettcher 1978; Obata et al. 1986; Wallace and Green 1991; Dyar et al. 1992a, 1992b; Oba 1997; Ernst and Liu 1998).

Several geochemical and mineralogical studies on amphiboles have been focused on mineral analyses and H isotope behavior (e.g., Graham et al. 1984; Bryndzia et al. 1990; Deloule et al. 1991). Crystallographic studies of the kaersutite structures and compositions have been carried out by several authors (e.g., Pechar et al. 1989; Popp et al. 1990, 1995a, 1995b, 2006; Young et al. 1997; King et al. 1999a). Investigations on metasomatized upper mantle xenoliths and associated megacrysts suites indicate that metasomatism is associated with distinctive sets of high ferric percentages in upper mantle mineral phases and suggest an interrelationship between Fe^{3+} and H^+ in these minerals (Wood and Virgo 1989; McGuire et al. 1989, 1991; Dyar et al. 1989, 1992a, 1992b, 1993; Popp et al. 1995a, 1995b; Young et al. 1997; King et al. 1999a; Gunter et al. 2003).

Mössbauer spectroscopy of minerals is an established technique that provides precise, highly reproducible Fe^{2+}/Fe^{3+} ratios and yields quantitative information about Fe^{2+} and Fe^{3+} site occupancy (Dyar 1984). Hawthorne (1983) and Gunter et al. (2003) summarized numerous Mössbauer studies of amphibole sample from the literature. However, there are few existing analyses of mantle kaersutite for which Fe^{3+} has been measured (e.g., Schwartz and Irving 1978; McGuire et al. 1989; Dyar et al. 1993; Popp et al. 1995b, 2006), and only little is known about the Mössbauer spectra of upper mantle oxy kaersutite. Because routine electron microprobe analyses do not give direct data on ferric/ferrous ratios of amphiboles, recourse has been made to calculations of valence states from simple assumptions on stiochiometry. Problems and major drawbacks of such calculations have been extensively discussed (e.g., Droop 1987; Deer et al. 1997; Schumacher 1991, 1997).

This paper presents the results of a study of upper mantle ferrikaersutite megacrysts hosted in scoria cones from the Harrat Ash Sham volcanic field (Fig. 1), using Mössbauer spectroscopy, H_2O, and microprobe analysis. We then discuss the implications of the findings for the origin of these ferrikaersutite megacrysts in relation to mantle oxygen fugacity and metasomatism.

PETROGRAPHY

The megacrysts and associated upper mantle xenoliths occur in Tertiary to Quaternary alkali olivine basalts and basanites of the Harrat Ash Sham volcanic field. The dominant megacryst phases in the Harrat Ash Sham Volcanic field are Al-clinopyroxene, Al-bronzite, pleonaste spinel, and kaersutite amphibole (Nasir 1995). Major and trace element partitioning in these megacrysts indicates that most of the megacrysts may have been in equilibrium with their host magmas at high pressure (Nasir 1995). The megacrysts are distinct in their petrography and chemistry from minerals in the associated Cr-diopside lherzolite xenoliths**,** but are similar in their chemistry to minerals of the Al-rich augite xenolith group (Nasir 1995). Several kaersutite megacrysts were collected from the scoria cone of the Tertiary Dhanoon volcano in the Harrat Ash Shama alkaline volcanic field (Fig. 1). Five representative megacrysts (KM1, KM2, KM3, KM4, and KM5) were selected for this study. Kaersutite

* E-mail: sobhi@squ.edu.om

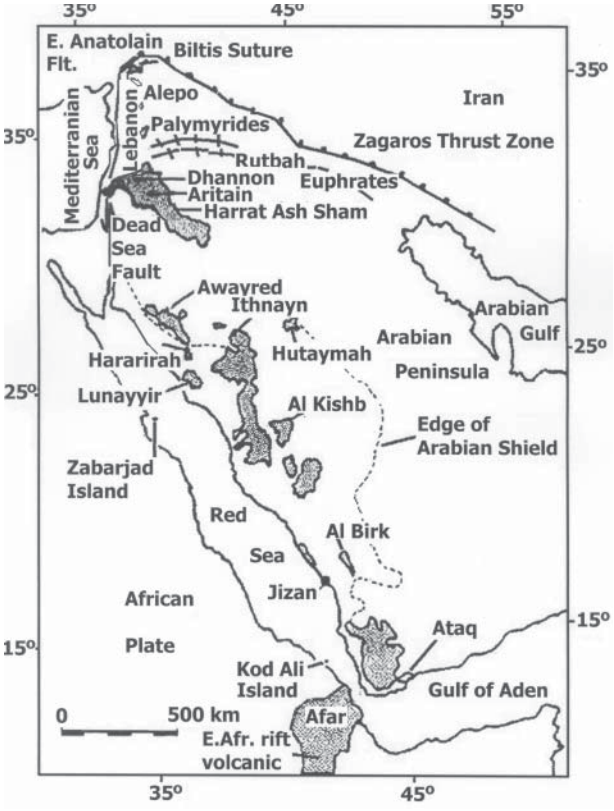

FIGURE 1. Location map of the investigated megacrysts showing Harrat Ash Sham volcanic field. Shaded fields represent Tertiary basalts.

megacrysts occur as black and hypidiomorphic to idiomorphic crystals with well-developed faces. They range in size from 5 × 3 × 3 cm to 10 × 5 × 5 cm. According to the irregular but even surface of these megacrysts, they were marginally melted or at least affected by resorption processes. Under the petrographic microscope, the kaersutites are strongly pleochroic, varying from deep reddish brown to yellow brown to pale brown and show perfect cleavage. The megacrysts contain several generations of solid mineral and melt inclusions, which may be compositionally and texturally produced by liquid immiscibility and by different stages of crystal growth (Nasir et al., in review). The inclusions occur in spherical, cylindrical and droplet shapes, and makeup 0.2–0.5 vol% of the megacryst. They are up to 0.8 mm in diameter, but the majority shows fairly constant sizes around 100 μm in diameter (Fig. 2). In case of elongated inclusions, the long axes of neighboring rods are oblique to the (110) cleavage planes of the host amphiboles. In many cases, inclusions are connected by veins containing the same mineral phases as the inclusions themselves. These veins are interpreted as former cracks that partly follow the kaersutite cleavage planes. The different types of melt inclusions in the kaersutite samples all show intensive red internal reflections with reflected light and are red in transmitted light pointing to the presence of oxidized iron and alteration. The inclusions have extremely variable phase proportions as well as melts of contrasting compositions (silica-sulfide-iron oxide). Solid daughter minerals in the inclusions are magnetite, hematite, pseudobrookite, pyrrhotite, chalcopyrite, Ni-Co-Fe-

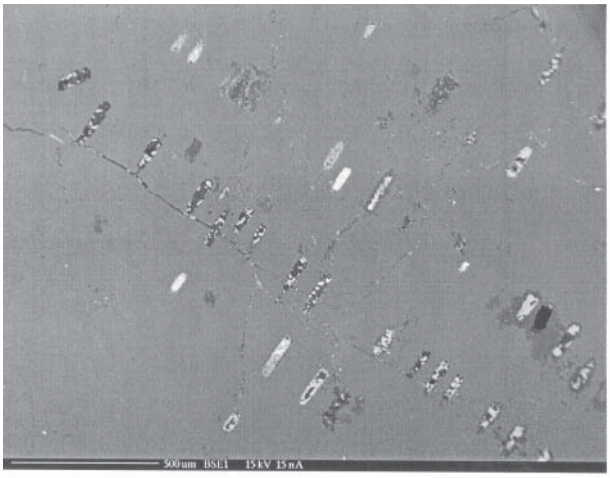

FIGURE 2. BSE image showing solid and melt inlusions within the kaersutite. White color within the inclusion is pyrrhotite; dark gray is hematite; light gray is magnetite.

monosulfide solid solution, diopside, augite, enstatite, olivine, plagioclase, phlogopite, and tschermakitic hornblende. Highly oxidized inclusion assemblages comprising frothy hematite, brownish silicate melt, and minor trevorite occur in conjunction with open cavities. The interior of oxide phase drops in the kaersutite samples is often frothy and foam-like impregnated by tiny holes representing gas cavities. Similar frothy hematite globules were also observed, for instance by Larocque et al. (2000), who interpreted these structures as degassing phenomenon. However, no gas or fluid phase has been observed to be associated with the studied inclusions. The inclusions are secondary and suffered several post trapping modification and oxidation during ascent to the surface. Textures and melt and solid mineral chemistry indicate that the inclusions formed through separations of an immiscible Fe-S-O melt, and subsequent formation and oxidation of separate Fe-S and Fe-O melts from a Fe-Ni-S-volatile-rich silicate melt at magmatic temperatures and pressures (Nasir et al. in review).

The observed phase relations (spinel peridotite) and thermobarometric calculations (e.g., 2 pyroxenes, Ca in orthopyroxene thermometers, Ca in olivine barometer) indicate that the megacrysts and associated xenoliths are crystallized from their parent melts at pressure of 12–15 kbar and temperature of 900–1050 °C, i.e., in the upper mantle or near the crust-mantle boundary (Nasir 1992, 1995; Nasir and Safarjalani 2000).

EXPERIMENTAL METHODS

All amphibole samples were analyzed by electron microprobe microanalysis and Mössbauer spectroscopy. The water content was determined by Karl-Fisher titration after vacuum extraction as well as by the Penfield method. The results of both methods have been tested against Equation 5 of King et al. (1999a). The Karl-Fisher titration technique yielded unreasonable results, which are possibly biased by the low H_2O content of the samples. In comparison, the Penfield method yielded reasonable results and is adopted in this study. The samples were dried under vacuum for 12 h at 90 °C. One gram of each sample was mixed with 2 g PbO. The mixtures were then fused in Penfield glass tube to liberate structural H_2O. Dry ice was used to condensate water vapor in the tube. The tube was then fused and weighed with liberated water, dried, and then weighed again. H_2O was determined by weight loss. The major error source for H_2O content is in weighing and is estimated to be minor (<5% of total wt% H_2O). Mineral analyses were carried out at Stuttgart University using the wavelength-dispersive system of a CAMECA SX100

electron microprobe. Operating conditions were: 15 kV accelerating voltage, 10 to 15 nA beam current and an integration time of 20 s on peak and on background. The raw data were corrected using the PAP procedure. The estimated analytical errors are ±0.5 to 1% for major elements and ±5 to 10% for minor elements. The microprobe analyses given in Table 2 are average of 10–20 analytical points. The megacrysts were found to be homogeneous. Ni, Cr, V, Zn, and Cl were not detected. The standards applied were corundum (A1), albite (Na), wollastonite (Ca, Si), MgO (Mg), orthoclase (K), rhodonite (Mn), hematite (Fe), barite (Ba), rutile (Ti), NiO (Ni), Cr_2O_3 (Cr), CoO (Co), spalerite (Zn), and chalcopyrite (Cu, Fe).

Samples were prepared for Mössbauer measurements by grinding them in a mortar and pestle under acetone to avoid oxidation. Mössbauer spectra were taken at 298 K employing transmission geometry using a 50 mCi, ^{57}Co/Rh source at Sultan Qaboos University. A simple spectrometer interfaced to a PC computer is used for collecting the data. The data were fitted by selecting the positions and intensities of the Lorentzian lines of every Gaussian component; all other parameters were kept fixed. The center shifts of the doublets were then fitted assuming no coupling to the quadropule splitting. Finally the width of the Gaussians components was fitted. All parameters were allowed to vary during the final fits. The detection limit is estimated to be ~2% Fe^{3+}/Fe_{tot}.

Results and discussion

The Mössbauer results for the kaersutite samples are reported in Table 1, together with selected reference data for similar upper mantle kaersutite. Figure 3 shows the fitted Mössbauer spectra. All spectra show a relatively similar pattern. Only two sharp absorption doublet lines, one having a quadrupole splitting at 0.73–0.87 mm/s and the other at 1.28–1.44 mm/s, could be visually identified. The isomer shift for the doublets varies between 0.39–0.41 mm/s for the first and between 0.38–0.39 mm/s for the second doublet. The line width varies between 0.39–0.48 and 0.45–0.54 mm/s for the first and the second doublet, respectively. The Mössbauer data for the doublets are consistent with Fe^{3+} and the quadrupole splitting attributes the two doublets to an octahedral site. Similar doublets have been assigned by Dyar et al. (1993) to $^{[M1]}Fe^{3+}$ and $^{[M2,M3]}Fe^{3+}$, respectively (cf. Table 1). There were no features indicative of Fe^{2+}.

According to Hawthorne (1981) and Redhammer and Georg (2002), trivalent cations prefer the M2 site in amphibole. However, the most intense Fe^{3+} component (61–68% Fe^{3+}) with quadrupole splitting 0.83–0.87 (sample KM2 to KM5) occurs in the M1 site, whereas the other Fe^{3+} component with quadrupole splitting 1.37–1.44 mm/s and intensity of 32–39% Fe^{3+} was assigned to the M2-3 site, following the site assignments proposed by Goldman (1979) and Dyar et al. (1993). Sample KM1 shows the opposite situation, where Fe^{3+} in the M2 site is more intense (63% Fe^{3+}). This sample has the lowest Fe^{3+} content (0.81 apfu) and the highest Mg and OH^- content (3.29 and 0.47 apfu, respectively). The experimental work of Phillips et al. (1988) found that some trivalent cations in M2 might relocate to M1 or M3 as oxidation occurs. The samples KM2 to KM5 contain more Fe^{3+} (1.02–1.13 apfu) and less OH^- (0.1–0.28 apfu) than the sample KM1. Dyar et al. (1993) presented several Mössbauer data of similar kaersutite megacrysts from different parts of the world. They found only one sample (Fr-12) with Mössbauer and chemical data similar to our samples (Table 1).

Table 2 compiles the results of microprobe analyses, Mössbauer spectroscopy, and H_2O analyses and the resulting stiochiometry based on normalization to 24 oxygens. The kaersutite host crystals are homogeneous in composition. No significant chemical zoning has been detected, even on the centimeter scale. According to Leake et al. (1997) the term "ferri" should be used for amphiboles with >1.0 Fe^{3+}, so all of the samples except KM1 (0.81 apfu) are ferrikaersutite, whereas sample KM1 can be classified as Fe^{3+}-rich kaersutite.

Figure 4a shows an inverse correlation between OH^- and Fe^{3+}. A linear regression fit to the plot yields a line with a correlation coefficient of –0.99 and with a slope of –1.00, which agree with the results of earlier worker's finding that Fe^{3+} and OH contents are inversely related in mantle kaersutites (Dyar et al. 1993; Popp et al. 1995a, 1995b; King et al. 1999a). This relation means that all available Fe^{2+} has been quantitatively converted to Fe^{3+}, and that dehydrogeneation or oxidation was so extensive that all Fe^{2+} was converted to Fe^{3+} by H-loss from the amphibole megacryst via oxy-substitution ($Fe^{2+} + OH^- = Fe^{3+} + O_2 + 1/2H_2$) (Popp et al. 1990; Dyar et al. 1993; King et al. 1999a). It is obvious from the inverse correlation between OH^- and Fe^{3+} that the bulk of Fe^{3+} variation can be explained by the relationship representing the oxy-substitution. Similar results were found by Dyar et al.

Table 1. Mössbauer results for the kaersutite samples in comparison to Mössbauer data from the literature

Sample no.	Valence and site assignment		IS (mm/s)	QS (mm/s)	LW (mm/s)	Area (%)
KM1	Fe^{3+}	M1	0.399 ± 0.030	0.733 ± 0.043	0.392 ± 0.056	37 ± 8
	Fe^{3+}	M2-3	0.384 ± 0.036	1.283 ± 0.059	0.539 ± 0.059	63 ± 7
KM2	Fe^{3+}	M1	0.400 ± 0.024	0.871 ± 0.030	0.487 ± 0.027	64 ± 3
	Fe^{3+}	M2-3	0.385 ± 0.300	1.447 ± 0.045	0.455 ± 0.043	36 ± 4
KM3	Fe^{3+}	M1	0.395 ± 0.021	0.876 ± 0.020	0.459 ± 0.021	68 ± 3
	Fe^{3+}	M2-3	0.385 ± 0.030	1.510 ± 0.043	0.465 ± 0.49	35 ± 4
KM4	Fe^{3+}	M1	0.416 ± 0.026	0.830 ± 0.035	0.472 ± 0.031	61 ± 5
	Fe^{3+}	M2-3	0.395 ± 0.034	1.388 ± 0.053	0.483 ± 0.050	39 ± 7
KM5	Fe^{3+}	M1	0.411 ± 0.025	0.859 ± 0.031	0.483 ± 0.026	61 ± 4
	Fe^{3+}	M2-3	0.380 ± 0.030	1.370 ± 0.045	0.479 ± 0.039	39 ± 5
Massif Central, France (Fr-12)	Fe^{3+}	M1	0.4	0.7	0.34	24
Dyar et al. (1993)	Fe^{3+}	M2	0.38	1.56	0.44	23
	Fe^{3+}	M3	0.4	1.16	0.46	53
Harrat Al Kishb, Saudi Arabia						
Dyar et al. (1993)	Fe^{3+}	M1	0.38	0.71–0.75	0.49–0.54	29–41
	Fe^{2+}	M1	1.12–1.13	1.96–2.02	0.37–0.4	32–38
	Fe^{2+}	M2-4	1.13–1.14	2.48–2.54	0.3–0.35	23–35
Harrat Hutaymah, Saudi Arabia						
Dyar et al. (1993)	Fe^{3+}	M1	0.39–0.4	0.79–1.31	0.42–0.59	28–50
	Fe^{2+}	M1	1.11–1.15	1.92–2.08	0.23–0.45	3–44
	Fe^{2+}	M2-4	1.09–1.14	2.4–2.59	0.27–0.30	4–32
Sodic amphiboles						
Ernst and Wai (1970)	Fe^{3+}	M2	0.35–0.48	0.42–0.50		
Sokolova et al. (2001)	Fe^{3+}	M2	0.35–0.48	0.48		

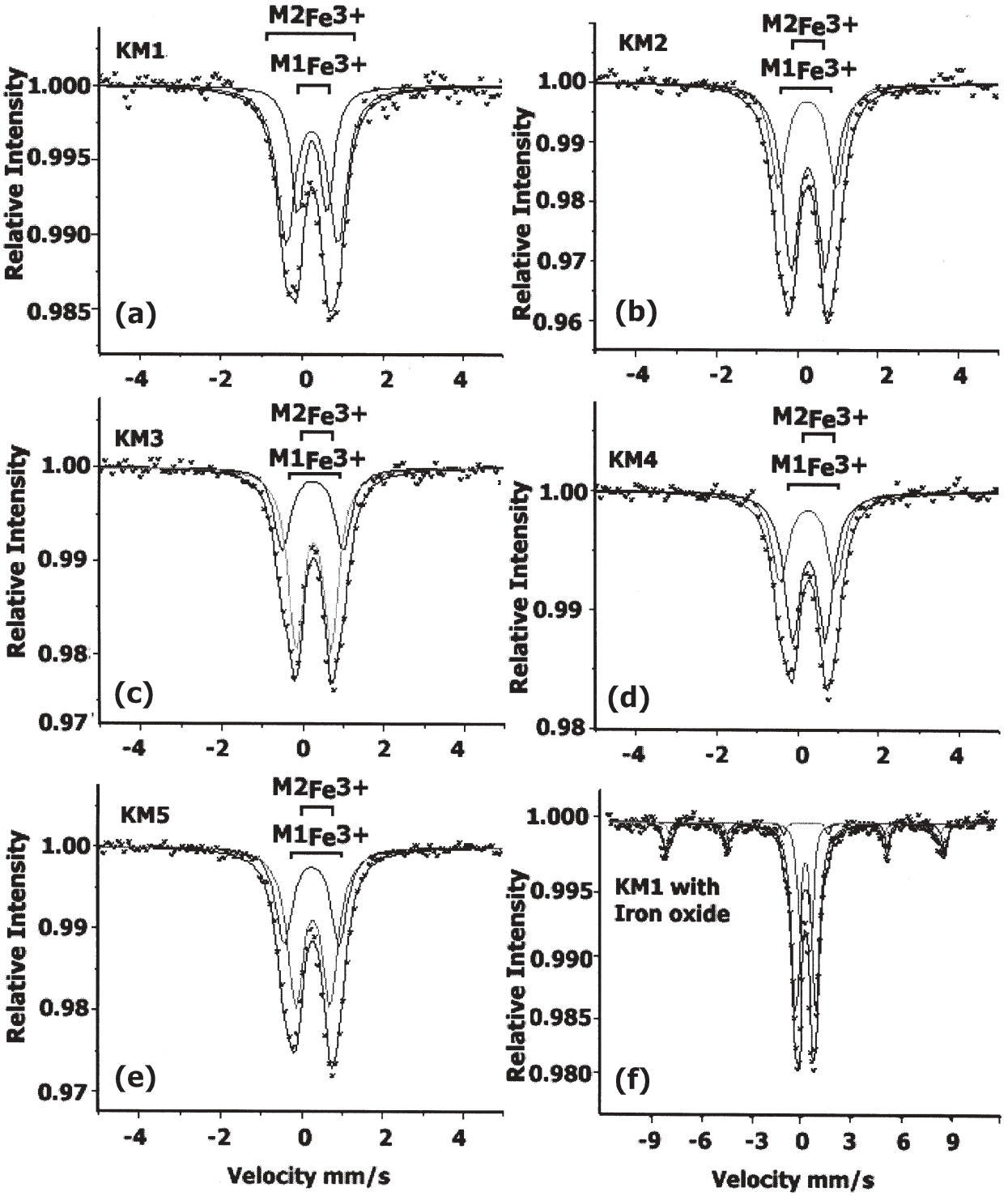

FIGURE 3. Mössbauer spectra of ferrikaersutite taken at room temperature: (**a–e**) kaersutite samples KM1 to KM5; (**f**) concentrated hematite inclusions within the sample KM1.

(1993), Popp et al. (1995a) and King et al. (1999a). Figure 4b shows that Fe^{3+} content correlates with OH + F + Cl + Ti (apfu) content (r^2 = –0.94, slope = –0.73). This relation was used by Popp et al. (1995a) to determine a model for Fe^{3+} calculation (Fe^{3+} = 2 – OH – Ti – F). Fig. 5 shows that the overall OH^- content correlates well with (Fe^{3+} + Ti + Al^{VI}) (r^2 = –0.99, slope = –0.79). This correlation was derived by King et al. (1999a, Eq. 5 therein) to calculate Fe^{3+} contents of a kaersutite if OH, Ti, Al,

TABLE 2. Chemical composition of the analyzed samples by electron microprobe, Mössbauer spectroscopy, and H_2O normalized to 24 O atoms

Sample	KM1	KM2	KM3	KM4	KM5
wt%					
SiO_2	40.83	40.68	40.54	39.17	40.78
TiO_2	6.25	5.58	5.44	6.94	5.71
Al_2O_3	14.31	14.85	14.65	15.09	14.46
Cr_2O_3	0.0	0.0	0.0	0.0	0.0
FeO_{tot}	7.34	9.98	10.85	9.12	10.12
MnO	0.05	0.06	0.05	0.07	0.04
MgO	15.05	13.13	12.85	13.22	13.18
CaO	11.06	10.59	10.33	11.53	10.43
Na_2O	2.51	2.77	2.62	2.59	2.63
K_2O	1.42	1.61	2.04	1.35	2.11
H_2O^*	0.48	0.16	0.10	0.28	0.14
F^-	0.1	0.07	0.12	0.1	0.1
Total	99.4	99.48	99.59	99.46	99.69
Fe^{3+}/Fe_{tot}‡	1	1	1	1	1
T-site					
Si	5.984	6.012	6.018	5.802	6.034
Al	2.016	1.988	1.982	2.198	1.966
Total	8.000	8.000	8.000	8.000	8.000
C-site					
Al	0.412	0.599	0.581	0.436	0.556
Ti	0.689	0.621	0.608	0.774	0.636
Fe^{3+}	0.810	1.110	1.212	1.017	1.127
Mg	3.089	2.670	2.599	2.773	2.681
Fe^{2+}	0.000	0.000	0.000	0.000	0.000
Mn	0.000	0.000	0.000	0.000	0.000
Tal	5.000	5.000	5.000	5.000	5.000
B-site					
Mg	0.199	0.223	0.245	0.147	0.227
Mn	0.001	0.008	0.006	0.009	0.005
Ca	1.737	1.677	1.643	1.830	1.654
Na	0.063	0.092	0.106	0.014	0.114
Total	2.000	2.000	2.000	2.000	2.000
A-site					
Na	0.650	0.702	0.648	0.730	0.638
K	0.266	0.303	0.386	0.255	0.398
Tal	0.916	1.005	1.034	0.985	1.036
F^-	0.046	0.033	0.056	0.047	0.047
OH^-	0.469	0.158	0.099	0.277	0.138
O^{2-}	1.485	1.809	1.845	1.676	1.815

* Determined by the Penfield method.
‡ Mössbauer spectroscopy.

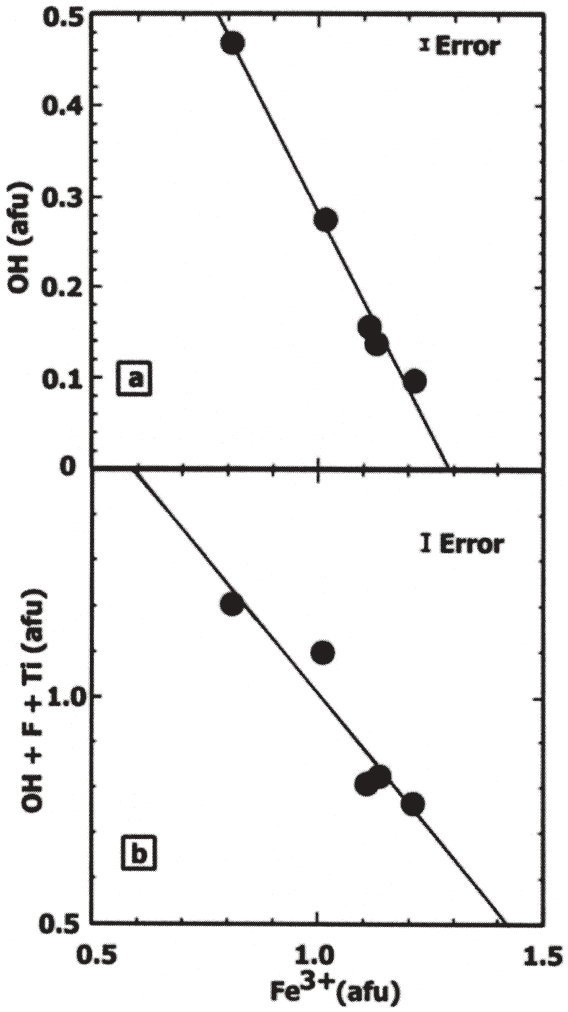

FIGURE 4. (**a**) Measured Fe^{3+} vs. OH content (apfu based on a 24 oxygen amphibole formula) for the kaersutite samples showing oxysubstitution mechanism for amphibole as suggested by Popp et al. (1990) ($r^2 = -0.99$, slope = –1). (**b**) Measured Fe^{3+} vs. OH + F + Ti content (apfu), ($r^2 = -0.94$, slope = –0.73). This relationship was used by Popp et al. (1995a) to determine a model for Fe^{3+} calculation.

and F contents are known. We did not observe any correlation in the studied samples that suggests a role for A-site or alkali element substitutions (figures not shown).

IMPLICATIONS FOR MANTLE METASOMATISM AND OXYGEN FUGACITY

Hops et al. (1992) proposed a model of megacryst formation from localized melt segregations at discrete episodes within the lithosphere, and suggested that reactions between lithospheric wall rocks and megacryst magma would enhance lithospheric metasomatism. Crystallization of megacrysts from these magmas within the lithosphere would promote an evolution of volatile-rich fluids, which are probably responsible for the production of kaersutite and phlogopite. Streaming of this evolved volatile flux may lead eventually to cracking of the lithosphere and extrusion of alkali basalts and accidental entrainment of xenoliths and megacrysts (Nasir 1995). However, sources of amphibole megacrysts could include metasomatically derived melts (Ionov et al. 1997), mantle cumulates and dikes (Irving 1974) and basaltic host melt (Green and Hibberson 1970).

The mineral phases in the typical upper mantle mineralogy (ol, opx, cpx, sp ± gt) have low ferric iron contents (e.g, Blundy et al. 1991; Woodland et al. 1999; McCammon et al. 2001). However, upper mantle kaersutite megacrysts have been reported with 0.27–0.50 Fe^{3+}/Fe_{tot} from Saudi Arabia (Mössbauer analyses; McGuire et al. 1989; Dyar et al. 1993), and with 0.26–0.98 Fe^{3+}/Fe_{tot} from Dish Hill (wet-chemical analyses; Wilshire and Trask 1971; Boettcher and O'Neil 1980) and with 0.48–0.93 Fe^{3+}/Fe_{tot} from the Grand Canyon (Best 1970). In comparison, the studied megacrysts and kaersutite sample Fr-12 from the Massif Central, France (Dyar et al. 1993) are among the most ferric-rich compositions recorded. Mattioli et al. (1989) suggested that patent metasomatism, which introduces ferric-rich amphibole, might lead to greater enrichment of bulk Fe^{3+} and an apparent greater metasomatic redox effect. Redox conditions (f_{O_2} and Fe^{3+}/FeO_{tot}) determine the stability of C-O-H-S fluid and solid phases in the mantle. King et al. (1999b) found that amphibole

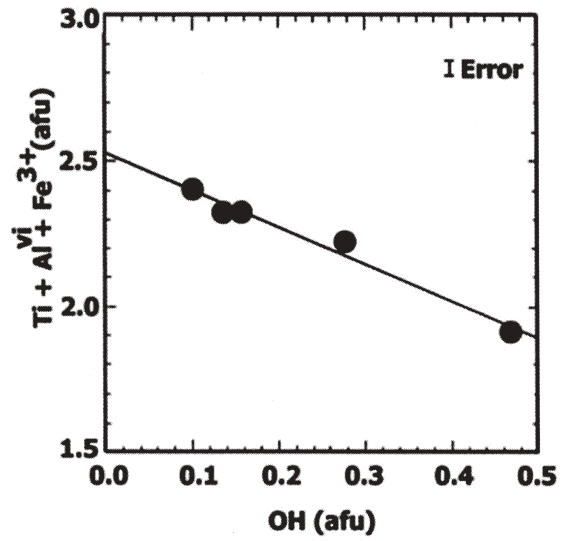

FIGURE 5. Measured OH vs. Ti + Al^{vi} + Fe^{3+} content (apfu), (r^2 = –0.99, slope = –0.79). King et al. (1999a) used this relation to calculate Fe^{3+} for samples with known OH content.

Fe^{3+}/Fe$_{tot}$ content increases and H decreases with increasing f_{O_2} and decreasing f_{H_2}. Also they found that amphibole H contents correlate with emplacement mechanism, with the most variable H contents found at lava flows and scoria cones (e.g similar to the Harrat Ash Sham volcanic field). At such localities, amphibole dehydrogenation likely occurs at the surface or en route to the surface (see discussion by King et al. 1999a, 1999b). However, Dyar et al. (1993) found that dehydrogenation of hornblende during transport seems unlikely to explain the entire ranges of H$^+$ and Fe^{3+} observed in their hornblende suite, as only limited H loss is possible by this mechanism. Total dehydrogenation and oxidation of the megacrysts would require time scales significantly longer than what is expected for transport (Dyar et al. 1993).

The Fe^{3+} contents of spinels from associated upper mantle lherzolite xenoliths from the Harrat Ash Sham have been determined using ^{57}Fe Mössbauer spectroscopy (Nasir et al. 1992, 1993). The determined Fe^{3+} fractions in spinel (Fe^{3+}/Fe$_{tot}$= 0.16–0.26) were used to calculate oxygen fugacity. The calculated f_{O_2}-*T*-*P* conditions are consistent with derivation of the lherzolite samples from a relatively oxidized source region dominated by CO_2 and/or H_2O fluid species. Calculated f_{O_2} values range from 0.5 up to 1.1 log units below the fayalite-magnetite-quartz (FMQ) buffer. The average Δf_{O_2} (relative to FMQ) is –0.29 log units, which is more oxidized than the average Δf_{O_2} calculated for upper mantle xenoliths from western Europe (–0.89; O'Neill and Wall 197), British Columbia (–1.05; Canil et al. 1990), and eastern Australia (–1.78; O'Neill and Wall 1987). The average Δf_{O_2} of the lherzolite samples from the Harrat Ash Sham is also more than the average Δf_{O_2} (relative to FMQ) for abyssal peridotite (–0.9; Bryndzia and Wood 1990), Ronada orogenic massif (–1.1; Woodland et al. 1992), and Semail harzburgite massif (–1.11; Nasir 1996). The investigated kaersutites have higher Fe^{3+} contents than similar kaersuitite megacrysts and associated phases from the central parts of the Arabia plate (e.g., Harrat Al Kishb and Hutaymah, cf. Fig. 1, Table 1 in this work). The high ferric contents in kaersutite and the high oxygen fugacity in associated lherzolite xenoliths suggest that the metasomatic fluid that crystallized these amphiboles imprinted the high Fe^{3+}/FeO$_{tot}$ ratio to the "dry" lherzolite mineralogy (i.e., spinel). This is also supported by the mineral phases of the minute globules and inclusions within the studied kaersutite megacrysts (e.g, hematite, pseudobrookite, and magnetite). All samples contain variable amounts of hematite inclusions as clearly overlapped with kaersutite spectrum in the Fe^{3+} field (e.g., Fig. 3e). The Mössbauer spectra in a handpicked powder sample show evidence for the presence of hematite. A typical spectrum consists of sextets from Fe in different sites (Fig. 3e). Petrographic and mineral-chemical relationships observed in the upper mantle xenoliths of the Arabian Tertiary volcanic fields plate have been interpreted as the result of metasomatism through infiltration of the mantle by basaltic magmas (Altherr et al. 1990; Henjes-Kunst et al. 1990; Nasir 1992, 1994; Nasir and Safarjalani 2000).

ACKNOWLEDGMENTS

We are grateful for thoughtful reviews by Darby Dyar, R. Popp, and anonymous reviewer. We acknowledge M. El Zain and A. Gismealsead for assistance with sample preparation and reading of the manuscript. T. Theye assisted with electron microprobe analysis.

REFERENCES CITED

Allen, J.C. and Boettcher, A.L. (1978) Amphibole in andesite and basalt: II Stability as a function of *P*-*T*-f_{H_2O}-f_{O_2}. American Mineralogist, 63,1074–1087.

Altherr, R., Henjes-Kunst, F., and Baumann, A. (1990) Asthenosphere vs. lithosphere as possible sources for basaltic magmas erupted during formation of the Red Sea: constraints from Sr, Pb, and Nd isotopes. Earth Planetary Science Letters, 96, 269–286.

Best, M.G. (1970) Kaersutite-peridotite inclusions and kindred megacrysts in basanitic lavas, Grand Canyon, Arizona. Contributions to Mineralogy and Petrology, 27, 25–44.

Blundy, J.D., Brodholt, J.P., and Wood, B.J. (1991) Carbon-fluid equilibria and the oxidation state of the upper mantle. Nature, 349, 321–324.

Boettcher, A.L. and O'Neil, J.R. (1980) Stable isotope, chemical, and petrographic studies of high pressure amphiboles and micas: Evidence for metasomatism in the mantle source regions of alkali basalts and kimberlites. American Journal of Science, 280-A, 594–621.

Bryndzia, L.T. and Wood, B.J. (1990) Oxygen thermobarometry of abyssal spinel peridotite: The redox state and C-O-H volatile composition of the earth's sub-oceanic upper mantle. American Journal of Science, 290, 1093–116.

Bryndzia, L.T., Davis, A.M., and Wood, B.J. (1990) The isotopic composition (*D*) of water in amphiboles and the redox state of amphibole-bearing upper mantle spinel peridotites. Geological Society of America Abstracts with Programs, 22(7), A254.

Canil, D., Virgo, D., and Scarf, C.M. (1990) Oxidation state of mantle xenoliths from British Columbia, Canada. Contributions to Mineralogy and Petrology, 104, 453–462.

Deer, W.A., Howie, R.A., and Zussman, J. (1997) Rock-Forming Minerals, vol. 2B: Double chain silicates (2nd ed.), 764 p. The Geological Society Publishing House, Bath.

Deloule, E., Albarede, F., and Sheppard, S.M.F. (1991) Hydrogen isotope heterogeneities in the mantle from ion probe analysis of amphiboles from ultramafic rocks. Earth and Planetary Science Letters, 105, 543–553.

Droop, G.T.R. (1987) A general equation for estimating Fe^{3+} concentrations in ferromagnesian silicates and oxides from microprobe analyses, using stoichiometric criteria. Mineralogical Magazine, 51, 431–435.

Dyar, M.D. (1984) Precision and interlaboratory reproducibility of measurements of the Mössbauer effect in minerals. American Mineralogist, 69, 1127–1144.

Dyar, M.D., McGuire, A.V., and Ziegler, R.D. (1989) Redox equilibria and crystal chemistry of coexisting minerals from spinel lherzolite mantle xenoliths. American Mineralogist, 74, 969–980.

Dyar, M.D., McGuire, A.V., and Harrell, M.D. (1992a) Redox behavior in contrasting styles of metasomatism in the upper mantle. Geochimica et Cosmochimica Acta, 56, 2579–2586.

Dyar, M.D., McGuire, A.V., and Mackwell, S.J. (1992b) Fe^{3+}/H$^+$ and D/H in kaersutites: Misleading indicators of mantle source fugacities. Geology, 20, 565–568.

Dyar, M.D., Mackwell, S.J., McGuire, A.V., Cross, L.R., and Robertson, J.D. (1993) Crystal chemistry of Fe^{3+} and H$^+$ in mantle kaersutite: Implications for mantle metasomatism. American Mineralogist, 78, 968–979.

Ernst, W.G. and Liu, J. (1998) Experimental phase-equilibrium study of Al- and Ti-contents of calcic amphibole in MORB: A semiquantitative thermobarometer. American Mineralogist, 83, 952–969.

Ernst, W.G. and Wai, C.M. (1970) Mössbauer, infrared, X-ray, and optical study of cation ordering and dehydrogenation in natural and heat-treated sodic amphiboles. American Mineralogist, 55, 1226–1258.

Goldman, D.S. (1979) A reevaluation of the Mössbauer spectroscopy of calcium amphiboles. American Mineralogist, 64, 109–118.

Graham, E.M., Harmon, R.M., and Sheppard, S.M.F. (1984) Experimental hydrogen isotope studies: Hydrogen isotope exchange between amphibole and water. American Mineralogist, 69, 128–138.

Green, D.H. and Hibberson, W. (1970) Experimental duplication of conditions of precipitation of high pressure phenocrysts in basaltic magma. Physics and Earth Planetary Science International, 3, 247–254.

Gunter, M., Dyar, D., Twamley, B., Foit, F., and Cornelius, S. (2003) Composition, ($Fe^{3+}/\Sigma Fe$), and crystal structure of non-asbestiform and asbestiform amphiboles from Libby, Montana, U.S.A. American Mineralogist, 88, 1970–1978.

Hawthorne, F.C. (1981) Crystal chemistry of the amphiboles. In D.R. Veblen, Ed., Amphiboles and other hydrous pyriboles—mineralogy, 9A, p. 1–102. Reviews in Mineralogy, Mineralogical Society of America, Chantilly, Virginia.

——— (1983) The crystal chemistry of the amphiboles. Canadian Mineralogist, 21, 173–480.

Henjes-Kunst, F., Altherr, R., and Baumann, A. (1990) Evolution and composition of the lithospheric mantle underneath the western Arabian peninsula: Constraints from Sr-Nd isotope systematics of mantle xenoliths. Contribution to Mineralogy and Petrology, 105, 460–472.

Hops, J.J., Gurney, J.J., and Winterburn, P. (1992) Megacrysts and high temperature nodules from the Jagersfontein kimberlite pipe. Geological Society of Australia, 14, 759–770.

Ionov, D.A., Griffin, W.L., and O'Reilly, S.Y. (1997) Volatile-bearing minerals and lithophile trace elements in the upper mantle. Chemical Geology, 141, 153–184.

Irving, A.J. (1974) Megacrysts from the Newer basalts and other basaltic rocks of southeastern Australia. Geological Society of America, Bulletin 85, 1503–1514.

King, P.L., Hervig, R.L., Holloway, J.R., Vennemann, T.W., and Righter, K. (1999a) Oxy-substitution and dehydrogenation in mantle-derived amphibole megacrysts. Geochemica et Cosmochemica Acta, 62, 3635–3651.

King, P.L., Hervig, R.L., Holloway, J.R., and Delaney, J.S. (1999b) Partitioning of H and Fe^{3+}/Fe_{total}) between amphibole and basanitic melt as a function of oxygen fugacity. EOS Transaction of American Geophysical Union, 80, S358.

Larocque, A.C.L., Stimac, J., Keit, J.D, and Huminicky, M.A. (2000) Evidence for open-system behavior in immiscible Fe-S-O-liquids in silicate magmas: implications for contributions of metals and sulfur to ore-forming fluids. Canadian Mineralogist, 38, 1233–1249.

Leake, B.B., Woolley, A.R, Arps, C.E.S., Birch, WD., Gilbert, M.C., Grice, J.D., Hawthorne, P.C., Kato, A., Kisch, H.J., Krivovichev, V.G., Linthout, K., Laird, J., Mandarino, J.A., Maresh, v'W., Nickel, E.H., Rock, N.M.S., Schumacher, J.C., Smith, D.C., Stephenson, N.N., Ungaretti, L., Whittaker, E.J.W., and Youzhi, G. (1997) Nomenclature of amphiboles: report of the subcommittee on amphiboles of the International Mineralogical Association, Commission on New Minerals and Mineral Names. American Mineralogist, 82, 1019–1037.

Mattioli, G.S., Baker, M.B., Rutter, M.J., and Stolper, E. (1989) Upper mantle oxygen fugacity and its relationship to metasomatism. Journal of Geology, 97, 521–536.

McCammon, C.A., Griffin, W.L., and Shee, S.R. (2001) Oxidation during metasomatism in ultramafic xenoliths from the Wesselton kimberlite, South Africa: implications for the survival of diamond. Contributions to Mineralogy and Petrology, 141, 287–296.

McGuire, A.V., Dyar, M.D., and Ward, K.W. (1989) Neglected Fe^{3+}/Fe^{2+}ratios: A study of Fe^{3+} content of megacrysts from alkali basalts. Geology, 17, 687–690.

McGuire, A.V., Dyar, M.D., and Nielson, J.E. (1991) Metasomatic oxidation of upper mantle peridotite. Contributions to Mineralogy and Petrology, 107, 252–264.

Nasir, S. (1992) The lithosphere beneath the northwestern part of the Arabian plate Jordan: evidence from xenoliths and geophysics. Tectonophysics, 201, 357–370.

——— (1994) Geochemistry and petrogenesis of Cenozoic volcanic rocks from the northwestern part of the Arabian continental alkali basalt province (Jordan). Africa Geoscience Review, 1, 455–467.

——— (1995) Cr-poor megacrysts from the Shamah volcanic field, northwestern part of the Arabian plate. Journal of African Earth Science, 21, 349–357.

——— (1996) Oxygen thermobarometry of the Semail harzburgute massif, Oman and United Arab Emirates. European Journal of Mineralogy, 8, 153–163.

Nasir, S. and Safarjalani, A. (2000) Lithospheric Petrology and Geochemistry beneath the Northern Part of the Arabian Plate (Syria). Journal African Earth Science, 34, 223–245.

Nasir, S., Abu-Aljarayesh, I., Mahmood, S., and Lehlooh, A. (1992) Oxidation state of the upper mantle beneath the northwestern part of the Arabian lithosphere. Tectonophysics, 213, 359–366.

Nasir, S., Lehlooh, A., Abu-Aljarayesh, I., and Mahmood, S. (1993) Ferric iron in upper mantle Cr-spinel, A Mössbauer spectroscopic study. Chemie der Erde (Geochemistry), 53, 265–271.

Oba, T. (1997) The stability fields of kaersutite and its substitution of $R^{2+} + 2Si = Ti + 2Al^{IV}$. In A.K. Gupta, K. Onuma, and M. Arima, Eds., Geochemical studies on synthetic and natural rock systems, p. 126–139. Allied Publishers Ltd, New Delhi.

Obata, T., Yagi, K., and Hariya, Y. (1986) Stability relation of kaersutite, reinvestigated on natural and synthetic samples. Morphology and phase equilibria of minerals: IMA, 1982, 353–363.

O'Neill, H.St.C. and Wall, V.J. (1987) The olivine-orthopyroxene-spinel oxygen barometer, the nickel precipitation curve, and oxygen fugacity of the earth's upper mantle. Journal of Petrology, 28, 1169–1191.

Pechar, F., Fuess, H., and Joswig, W. (1989) Refinement of the crystal structure of kaersutite (Vlatbra, Bohemia) from neutron diffraction. Neues Jahrbuch fuer Mineralogie Monatshefte, 89(3), 137–143.

Phillips, M.W., Popp, R.K, and Clowe, CA (1988) Structural adjustments accompanying oxidation-dehydrogenations in amphiboles. American Mineralogist, 73, 500–506.

Popp, R.K., Phillips, M.W., and Harrell, J.A. (1990) Accommodation of Fe^{3+} in natural Fe^{3+}-rich calcic and subcalcic amphiboles: Evidence from published chemical analyses. American Mineralogist, 75, 163–169.

Popp, R.K., Virgo, D., and Phillips, M.W. (1995a) H deficiency in kaersutitic amphiboles: Experimental verification. American Mineralogist, 80, 1347–1350.

Popp, R.K., Virgo, D., Yoder, H.S., Jr., Hoering, T.C., and Phillips, M.W. (1995b) An experimental study of phase equilibria and Fe oxy-component in kaersutitic amphibole: Implications for the f_{H_2} and a_{H_2O} in the upper mantle. American Mineralogist, 80, 534–548.

Popp, R.K., Hibbert, H.A., and Lamb, W.M. (2006) Oxy-amphibole equilibria in Ti-bearing calcic amphiboles: Experimental investigation and petrologic implications for mantle derived amphiboles. American Mineralogist, 91, 54–66.

Redhammer, G.J. and Georg, R. (2002): Crystal structure and Mössbauer spectroscopy of the synthetic amphibole potassic-ferri-ferrorichterite at 298 K and low temperatures (80–110 K). European Journal of Mineralogy, 14, 105–114.

Schumacher, J.C. (1991) Empirical ferric iron corrections: Necessity, assumptions, and effects on selected geothermobarometers. Mineralogical Magazine, 55, 3–18.

——— (1997) Appendix 2: the estimate of ferric iron in electron microprobe analysis of amphiboles. European Journal of Mineralogy, 9, 643–651.

Schwartz, K.D. and Irving, AJ. (1978) Cation valence determinations in kaersutite and biotite megacrysts from alkalic basalts: Evidence for Ti^{4+} in the upper mantle. Eos, 59, 1214–1215.

Sokolova, E.V., Hawthorne, F.C., Gorbatova, V., McCammon, C., and Schneider, J. (2001) Ferrian winchite from Ilmen Mountains, Southern Urals, Russia and some problems with the current scheme of nomenclature. Canadian Minerlogist, 39, 171–177.

Wallace, M.E. and Green, D.H. (1991) The effect of bulk rock composition on the stability of amphibole in the upper mantle: Implications for solidus positions and mantle metasomatism. Contribution to Mineralogy and Petrology, 44, 1019.

Wilshire, H.G. and Trask, N.J. (1971) Structural and textural relationships of amphibole and phlogopite in peridotite inclusions, Dish Hill, California. American Mineralogist, 56, 240–253.

Wood, D.J. and Virgo, D. (1989) Upper mantle oxidation state: Ferric iron contents of lherzolite spinels by ^{57}Fe Mossbauer spectroscopy and resultant oxygen fugacities. Geochimica et Cosmochimica Acta, 53, 1277–1291.

Woodland, A.B. and Peltonen, P. (1999) Ferric iron contents of garnet and clinopyroxene and estimated oxygen fugacities of peridotite xenoliths from the Eastern Finland Kimberlite Province. In J.J. Gurney, J.L. Gurney, M.D. Pascoe, and S.H. Richardson, Eds., The P.H. Nixon Volume, Proceeding VII International Kimberlite conference, p. 904–911. Red Roof Design, Cape Town, South Africa.

Woodland, A.B., Kornprobst, J., and Wood, B.J. (1992) Oxygen thermobarometry of orogenic lherzolite massifs. Journal of Petrology, 23, 203–230.

Young, E.D., Virgo, D., and Popp, R.K. (1997) Eliminating closure in mineral formulae with specific application to amphiboles. American Mineralogist, 82, 790–806.

MANUSCRIPT RECEIVED OCTOBER 24, 2005
MANUSCRIPT ACCEPTED MARCH 5, 2006
MANUSCRIPT HANDLED BY DARBY DYAR